

## THE EVOLUTIONARY STATUS OF ISOLATED DWARF IRREGULAR GALAXIES II. STAR FORMATION HISTORIES AND GAS DEPLETION

LIESE VAN ZEE<sup>1</sup>

Herzberg Institute of Astrophysics, 5071 W. Saanich Rd,  
Victoria, British Columbia V9E 2E7, Canada

*to appear in The Astronomical Journal*

### ABSTRACT

The results of UBV and H $\alpha$  imaging of a large sample of isolated dwarf irregular galaxies are interpreted in the context of composite stellar population models. The observed optical colors are best fit by composite stellar populations which have had approximately constant star formation rates for at least 10 Gyr. The galaxies span a range of central surface brightness, from 20.5 to 25.0 mag arcsec<sup>-2</sup>; there is no correlation between surface brightness and star formation history. Although the current star formation rates are low, it is possible to reproduce the observed luminosities without a major starburst episode. The derived gas depletion timescales are long, typically  $\sim 20$  Gyr. These results indicate that dwarf irregular galaxies will be able to continue with their slow, but constant, star formation activity for at least another Hubble time.

The sample of isolated dIs is compared to a sample of star bursting dwarf galaxies taken from the literature. The star bursting dwarf galaxies have many similar properties; the main difference between these two types of gas-rich dwarf galaxies is that the current star formation is concentrated in the center of the star bursting systems while it is much more distributed in the quiescent dIs. This results in pronounced color gradients for the starbursting dwarf galaxies, while the majority of the quiescent dwarf irregular galaxies have minor or non-existent color gradients. Thus, the combination of low current star formation rates, blue colors, and the lack of significant color gradients indicates that star formation percolates slowly across the disk of normal dwarf galaxies in a quasi-continuous manner.

*Subject headings:* galaxies: dwarf — galaxies: evolution — galaxies: fundamental parameters — galaxies: irregular

### 1. INTRODUCTION

The dwarf irregular class contains galaxies with widely disparate physical properties; dwarf irregulars are usually classified as such based on appearance (irregular morphology) and an intrinsic low luminosity, but their luminosities span at least 3 orders of magnitude ( $\sim 10^6 - 10^9 L_{\odot}$ ), and current star formation rates span at least 4 orders of magnitude ( $\sim 0.001 - 1. M_{\odot} \text{ yr}^{-1}$ ). The wide range of current star formation rates is particularly puzzling: why do some dwarf galaxies appear to have extremely high current star formation rates, relative to their total mass, while others do not? Is a “starburst” phase common to all dwarf galaxies, so that dwarfs which currently have lower star formation rates are in a period of quiescence before (or after) an episode of vigorous star formation? In other words, is the tendency to burst an intrinsic property of the dwarf irregular class, or a phenomenon associated with only a subset of the class? If the former, then the disparate observed properties may be merely an artifact of detecting galaxies at different phases in a common star formation history, while the latter would suggest that the rarer starbursting dwarf galaxies are not representative of the class. In this paper, the results of UBV imaging, H $\alpha$  imaging, and neutral hydrogen measurements are used to investigate the star formation histories of a sample of isolated dwarf irregular galaxies which span a range of optical sizes, surface brightnesses, and current star formation rates, in order to

address the question of whether the majority of normal dwarf irregular galaxies have similar star formation histories, and to investigate whether these “typical” dwarf galaxies are related to the class of starbursting dwarfs.

The use of global optical colors as a tracer of star formation history is a well developed subject (e.g., Tinsley 1980). Recent improvements in galaxy evolution models have led to the ability to model composite stellar populations with a variety of star formation histories, stellar metallicities, and initial mass functions (e.g., Leitherer et al. 1996). Despite these advances, the results of galaxy evolution models for dwarf irregular galaxies are not significantly different than those first obtained 30 years ago. Three conceptually different schematic star formation histories are able to reproduce the observed optical colors of dwarf irregular galaxies: (1) constant star formation rates for approximately a Hubble time (e.g., Gallagher, Hunter, & Tutukov 1984; Hunter & Gallagher 1986); (2) recent elevated star formation rates superposed on an older stellar population (e.g., Searle et al. 1973; Huchra 1977) and (3) recent onset of star formation activity (e.g., Searle & Sargent 1972). The latter is similar to model (2), but has no underlying old stellar component; both (2) and (3) can be summarized as “burst” models, where the current star formation rate is significantly higher than the average past star formation rate. As one would expect for galaxies which are generally the bluest of the normal gas-rich galaxies, all of these models indicate that the dom-

<sup>1</sup>Visiting Astronomer, Kitt Peak National Observatories, which is operated by the Association of Universities for Research in Astronomy, Inc. (AURA) under a cooperative agreement with the National Science Foundation.

inant stellar populations in dwarf irregular galaxies are “young,” i.e., formed within the last Gyr or so. The underlying difference between these models is whether the current star formation activity is typical of the past star formation activity (constant star formation rate model), or if the current star formation rate is elevated over the past rate (burst model). Thus, to determine which of these models best fits the “typical” dwarf irregular galaxy, it is necessary to have additional information about the evolutionary status, such as the current star formation rate, gas mass fraction, and stellar and gaseous metallicities.

Systematic surveys of the current star formation activity in dwarf irregular galaxies have shown that galaxies selected on the basis of extreme blue colors (i.e., the blue compact dwarf galaxies) have unusually high current star formation rates, and thus are best described by bursting models (e.g., Searle & Sargent 1972; Marlowe et al. 1997; Almozno & Brosch 1998). In contrast, H $\alpha$  imaging of large samples of dwarf galaxies indicates most dwarf irregular galaxies have extremely low star formation rates, with only a few HII regions distributed sparsely across the optical disk (e.g., Strobel, Hodge, & Kennicutt 1991; Hunter et al. 1993; Miller & Hodge 1994; Miller 1996; Heller, Almozno, & Brosch 1999; Roye & Hunter 2000). However, the issue of whether these low star formation rates are representative of the typical star formation activity in these galaxies remains, since low star formation rates are also expected during the quiescent phase of an episodic starburst model.

On the theoretical side, early models of star formation activity in dwarf irregular galaxies indicated that small disks would be unstable to star formation activity. In particular, episodic bursts of star formation appeared to arise naturally from stochastic self-propagating star formation (SSPSF) models (Gerola et al. 1980). However, recent work on the gas distribution in normal and low surface brightness (LSB) dwarf galaxies indicates that the gas density is well below the threshold for star formation across the entire stellar disk, suggesting that it is difficult to initiate a global burst of star formation, even in intrinsically small galaxies (Hunter & Plummer 1996; van Zee et al. 1997c; Hunter, Elmegreen & Baker 1998). Thus, a more accurate representation of the star formation process in dwarf galaxies may be that of random percolation of star formation activity across the stellar disk. This picture is fundamentally different than classic SSPSF since the star formation activity does not propagate from one cell to another; rather, star formation occurs only in a few localized regions where the local gas density is sufficient to permit molecular cloud formation and subsequent star formation. The onset of star formation activity in this type of model is still a stochastic process, but the star formation activity across the galaxy is expected to be more quiescent since it is unlikely that the entire disk will have sufficient gas density to permit a sudden starburst.

One additional key factor is that these two models for star formation activity in dwarf galaxies predict different radial distributions for the composite stellar populations. Not only are the global star formation histories different (i.e., episodic starbursts vs. quasi-continuous star formation activity), but the local star formation histories will be different as well. In a starburst model, a region of the stel-

lar disk “turns on” simultaneously with a very high rate of star formation while the remainder of the disk (usually the outskirts) remains quiescent. This centralized star formation activity will result in a radial color gradient in starbursting systems (as observed by e.g., Papaderos et al. 1996b; Marlowe et al. 1997, 1999; Doublier et al. 1997, 1999). In contrast, a low level of star formation activity which percolates across the disk in a random manner will result in minor local color variations, but no large scale color gradient, provided that there is no favored location within the disk. Thus, one way to distinguish between a starburst model and a percolating star formation model is to investigate the spatial distributions of the composite stellar populations in dwarf galaxies.

Ideally, star formation histories should be derived directly from the distribution of resolved stars on a color-magnitude diagram (CMD), where the number of stars in each evolutionary phase can be used to infer the past star formation history (e.g., Tosi et al. 1991; Greggio et al. 1993; Marconi et al. 1995; Hunter & Thronson 1995; Tolstoy 1996; Dohm-Palmer et al. 1997, 1998; Lynds et al. 1998; Gallagher et al. 1998; Tolstoy et al. 1998; Greggio et al. 1998; Schulte-Ladbeck et al. 1999). However, most dwarf galaxies are too distant to make such an analysis feasible, even with the high spatial resolution of the *Hubble Space Telescope*. Thus, the present study relies on the integrated optical (UBV) colors in order to derive the star formation histories of a large sample of dwarf galaxies. The observations and data reduction of the sample are described in van Zee (2000, hereafter Paper I). As described in Paper I, the sample was selected to include isolated galaxies in order to minimize the possible effects of recent interactions on the star formation histories.

This paper is organized as follows. A brief summary of the sample selection and data acquisition and reduction is presented in Section 2 (see Paper I for full details). The observed colors are interpreted in the context of composite stellar populations in Section 3. Correlations between the current star formation rate and global parameters, such as gas mass fraction, are discussed in Section 4. Section 5 contains a brief summary of the conclusions.

## 2. OBSERVATIONS

The observations and data reduction for the UBV and H $\alpha$  images were discussed in Paper I. A brief summary of the sample selection and observational procedures are presented in this section.

### 2.1. Sample Selection

The UBV imaging sample was drawn primarily from the *Uppsala General Catalog of Galaxies* (Nilson 1973, UGC). All of the selected galaxies were classified as late-type spirals or irregular, with absolute magnitudes fainter than  $-18.0$ , and with heliocentric velocities less than  $3000 \text{ km s}^{-1}$ . Galaxies with known neighbors within  $30'$  and  $500 \text{ km s}^{-1}$  were excluded (nearer neighbors have subsequently been identified for some of the objects; see Paper I for more details). Projected distances between the target galaxies and their nearest known neighbor are on the order of  $100 - 200 \text{ kpc}$ , which translates into a crossing time of approximately  $1 \text{ Gyr}$ . Furthermore, the nearest known neighbor is not usually an extremely luminous system; most often, the neighboring system is another low

luminosity galaxy. Thus, the selection criteria result in a sample which contains low luminosity systems which are unlikely to have had significant interactions within the last several Gyr.

## 2.2. Optical Imaging

Optical images of the isolated dwarf galaxy sample were obtained with the Kitt Peak 0.9m telescope during 1996–1999. Full details of the observations and data reduction are presented in Paper I. Briefly, photometric images were obtained of 48 late-type galaxies in U, B, and V; H $\alpha$  images were obtained for 51 galaxies. The optical images were reduced following standard procedures. After sky subtraction and masking of the foreground stars, the apparent magnitudes and optical colors were measured.

The observed properties of the galaxies in the UBV imaging sample are tabulated in Table 1. This table contains: (1) UGC number; (2) an alternate name for the system; (3) morphological type from the RC3; (4) inclination angle as derived from the optical axial ratios at the lowest surface brightness level detected in the V-band images, assuming  $q_0 = 0.2$ ; (5) observed apparent B magnitude, corrected for Galactic extinction; (6) observed  $B-V$  color within a 25 mag arcsec $^{-2}$  aperture, corrected for Galactic extinction; (7) observed  $U-B$  color within the same aperture, corrected for Galactic extinction; (8) integrated HI flux density; (9) heliocentric velocity; (10) width of the HI line profile, measured at 20% of the peak; (11) derived  $M_H/L_B$ ; and (12) source of the tabulated HI data. The Galactic extinction correction was obtained from Schlegel et al. (1998), and is based on the dust distribution of the Milky Way. Since the internal extinction correction is uncertain for low metallicity galaxies, no correction was applied. The HI data were compiled from a variety of sources (Fisher & Tully 1981; Tift & Cocke 1988; Schneider et al. 1990, 1992; Giovanelli & Haynes 1993; Giovanelli et al. 1997; van Zee et al. 1997d; Haynes et al. 1998); data from recent observations and small telescopes (i.e., large beams) were favored in the final tabulation. In the few cases where  $W_{20}$  was not included in the published paper, the original HI data were obtained, and the width was remeasured at  $W_{20}$ .

Distances to most of the galaxies in this sample are uncertain. A few of the galaxies are near enough that distances have been measured directly: UGC 685 – Hopp (1999); UGCA 292 – Makarova et al. (1998); UGC 9128 – Aparicio et al. (2000); DDO 210 – Lee et al. (1999); UGC 12613 – Gallagher et al. (1998). For the remainder, the adopted distance was calculated from the HI recessional velocity, assuming a Hubble constant of 75 km s $^{-1}$  Mpc $^{-1}$  and using a nonlinear Virgocentric infall model based on the outline of Schechter (1980).

Distance dependent parameters are tabulated in Table 2. This table contains: (1) UGC number or other primary designation; (2) adopted distance; (3) absolute magnitude; (4) extrapolated central surface brightness for an exponential disk, corrected for Galactic extinction and inclination effects; (5) scale length of the exponential disk; (6) gradient in the  $B-V$  color; (7) gradient in the  $U-B$  color; (8) logarithm of the total HI mass; (9) current star forma-

tion rate; (10) the average past star formation rate; and (11) the gas depletion time scale. The current star formation rate was calculated from the observed H $\alpha$  luminosity, using the conversion factor from Kennicutt (1998):

$$SFR = 7.9 \times 10^{-42} L(H\alpha) \quad (1)$$

where  $SFR$  is the current star formation rate in solar masses per year and  $L(H\alpha)$  is the H $\alpha$  luminosity in erg s $^{-1}$ . The above conversion factor assumes a Salpeter (1955) initial mass function (IMF) and solar abundances, and is a slight ( $\sim 12\%$ ) increase in the SFR relative to the SFR conversion factor of Hunter & Gallagher (1986). The average past star formation rate was derived from the observed luminosity and the assumption that the galaxy has been forming stars for 13 Gyr; a complete description of the calculation of the average past star formation rate is presented in Section 3.4. The gas depletion time scale provides an indication of how long star formation can continue at the present rate before exhausting the fuel supply, and was calculated by taking the total mass of hydrogen and dividing by the current star formation rate.

## 2.3. Optical Spectroscopy of UGC 5205

Low resolution optical spectra of UGC 5205 were obtained at the Palomar 5m telescope<sup>3</sup> during the night of 1997 January 10. The observations were undertaken in a manner similar to those described in van Zee et al. (1998). Two 1200 sec exposures were obtained with the long slit centered on UGC 5205 and aligned along the parallactic angle ( $0^\circ$ ); the slit was 120'' in length, and a 2'' aperture was selected. The spectra were acquired with matched gratings on the blue and red sides of the Double Spectrograph, providing an effective resolution of 9.2 Å (2.19 Å/pix) for the blue camera and 7.8 Å (2.46 Å/pix) for the red camera. The final combined spectra provided complete spectral coverage from 3600–7600 Å. The night was non-photometric, but relative flux calibration was obtained by observations of spectrophotometric standard stars (Massey et al. 1988).

## 3. STAR FORMATION HISTORIES

The results of the UBV and H $\alpha$  imaging observations are used in this Section to derive approximate star formation histories. The global colors of the isolated dI sample are presented in Section 3.1. The stellar population models are described in Section 3.2. The global colors of the isolated dI sample and a comparison sample of starbursting dwarf galaxies are used to derive average star formation histories in Section 3.3. Finally, the star formation histories based on the global colors are checked for consistency with current and past star formation rates in Section 3.4.

### 3.1. Global Colors

The analysis presented in the subsequent sections is based primarily on the observed global colors. As mentioned in the Introduction, one of the fundamental differences between the two different models of star formation activity in dwarf galaxies is the possibility that starbursting dwarf galaxies will have substantial color gradients. Since a global color will only measure the luminosity

<sup>3</sup>Observations at the Palomar Observatory were made as part of a continuing cooperative agreement between Cornell University and the California Institute of Technology.

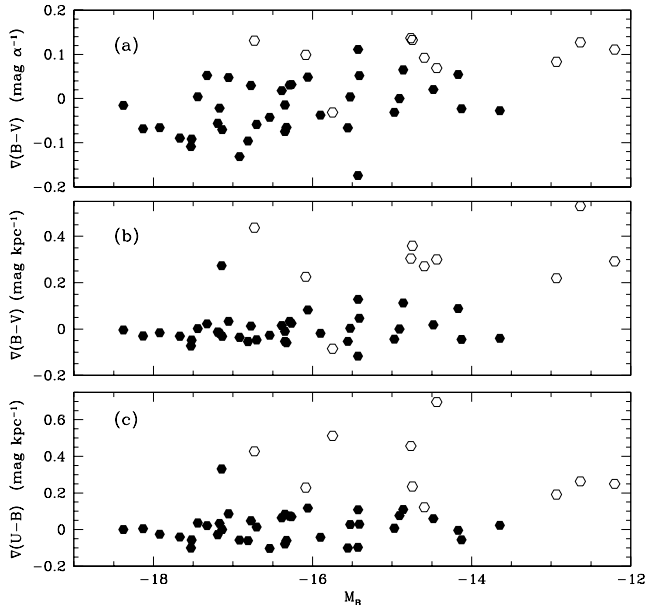


FIG. 1.— Observed color gradients in the dwarf irregular sample. (a) The  $B-V$  color gradient in units of exponential disk scale length; (b) the  $B-V$  color gradient in units of  $\text{mag kpc}^{-1}$ ; (c) the  $U-B$  color gradient in units of  $\text{mag kpc}^{-1}$ . Galaxies with small scale lengths ( $\alpha < 0.5 \text{ kpc}$ ) are shown with open symbols in all plots. Most of the dIs have negligible color gradients. However, the central regions of compact dIs are bluer than their outskirts.

weighted average of the dominant stellar population, any system with a substantial color gradient will be misrepresented by a global color.

The observed color gradients for the isolated dI galaxies are shown in Figure 1. The top panel shows the  $B-V$  color gradient in terms of exponential scale length ( $\text{mag } \alpha^{-1}$ ). Interestingly, if the  $B-V$  and  $U-B$  color gradients are shown in terms of a physical linear scale ( $\text{mag kpc}^{-1}$ ; Figure 1b,c), a handful of galaxies separate from the general trends. These galaxies are slightly redder in their outskirts, and, as a class, tend to have very short scale lengths for their luminosity. Given their small sizes and color gradients, these “compact dIs” may be related to the starbursting dwarf galaxies. Nonetheless, the net differences between the global colors and the colors for the inner and outer regions are minor since these galaxies are quite small; for example, assuming that the galaxian light has been traced to  $1.5 \alpha$  (approximately  $26.5 \text{ mag arcsec}^{-2}$  for this sample of galaxies), this corresponds to only  $\sim 0.15 \text{ mag}$  color difference between the inner to outer regions of the disk for the most extreme cases. Thus, it appears that the radial color gradients are negligible for the majority of galaxies in this sample.

The extinction corrected global colors of the isolated dwarf irregular galaxy sample are shown in Figure 2; the median colors for the sample are  $B-V = 0.42 \pm_{0.05}^{0.04}$  and  $U-B = -0.22 \pm_{0.07}^{0.04}$ . Also shown on Figure 2 are the optical colors for two fiducial galaxies: the Large Magellanic Cloud (LMC) (Hardy 1978) and HI 1225+01 (Salzer et al. 1991). The locations of these two galaxies on the UB $V$  color-color diagram illustrate the extreme range of colors found in dwarf irregular galaxies. The LMC is slightly more luminous than the class of object considered here, but, more importantly perhaps, its star formation history has almost certainly been influenced by interactions with

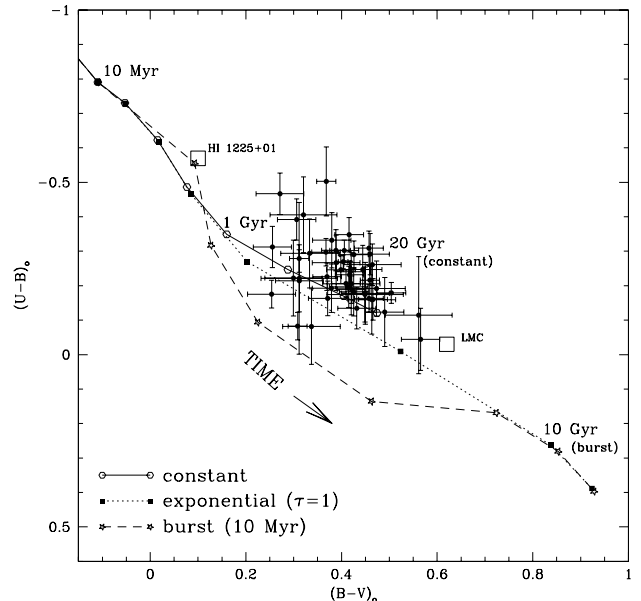


FIG. 2.— Color-color diagram of the isolated dwarf galaxy sample. Three evolution tracks for low metallicity (1/5 solar) composite stellar populations from the Bruzual & Charlot (1996) models are shown: a short (10 Myr) burst of star formation (long dashed lines); an exponentially decreasing star formation rate, with an e-folding time of 1 Gyr (short dashed lines); and a constant star formation rate (solid lines). The models are marked every 0.5 dex, and time increases from the upper left hand corner to the lower right hand corner. The short burst and exponentially decreasing star formation rates both result in a red galaxy after a Hubble time, while a constant star formation rate results in a blue system, similar to the observed properties of the dwarf irregular galaxies. Also shown are the global colors of HI 1225+01 (Salzer et al. 1991) and the LMC (Hardy 1978).

its near neighbor, the Milky Way. Detailed color-magnitude diagrams indicate that the star formation history of the LMC was somewhat “bursty” in nature [e.g., van den Bergh (1991); Girardi et al. (1995), but see also Holtzman et al. (1999)]. The slightly redder colors of the LMC are naturally explained if the LMC is in a predominantly quiescent phase after a major episode of star formation. At the other extreme, HI 1225+01 has much bluer colors than the typical dwarf irregular galaxy, and may be an example of a galaxy dominated by a young stellar population. While still controversial, it has been suggested that HI 1225+01 may be an example of a galaxy at the present epoch forming stars for the first time (Salzer et al. 1991).

Despite the large differences in colors between these two fiducial dwarf irregular galaxies, one remarkable aspect of the data shown in Figure 2 is that the majority of the isolated dwarf irregular galaxies have similar UB $V$  colors. In fact, the entire sample occupies only a small locus in the UB $V$  color-color diagram. Based on this remarkably small range of optical colors, it appears that the majority of isolated dwarf irregular galaxies have had similar star formation histories, with little dependence on total luminosity or surface brightness.

### 3.2. Composite Stellar Population Models

The goal of galaxy evolution modeling is to use the observed properties of the present composite stellar population to infer how the star formation rate varied with time. The models quickly become degenerate since the observed

colors provide only a luminosity weighted measure of the integrated light of the composite stellar populations. In particular, old (faint) stellar populations can be over shadowed by young (luminous) stellar populations; in addition, variations in either the initial mass function (IMF) or stellar metallicity can mimic changes in the star formation rate. Thus, in practice, it is necessary to determine not only the star formation history (SFH), but also how both the IMF and metallicity of the stellar population changed with time. Given these degeneracies, a plethora of galaxy evolution models can be found to fit any combination of colors, particularly if only a few bandpasses are observed. However, by restricting the possible star formation histories to simple variations of the star formation rate (an SFR which changes smoothly with time, or one with well defined starbursts, for example), it is possible to derive reasonable SFH models for galaxies with a wide range of colors (e.g., Larson & Tinsley 1978).

The galaxy evolution code of Bruzual & Charlot (1996) (BC96, hereafter) was used to investigate color evolution tracks for a variety of possible star formation histories and stellar metallicities. The BC96 galaxy evolution code is an improved version of the composite stellar population models originally described in Bruzual & Charlot (1993). As in Bruzual & Charlot (1993), the mono-metallicity composite stellar populations are built through the synthesis of stellar evolutionary tracks (e.g., Lejeune et al. 1997). The version of the galaxy evolution code run here includes options for sub- and super-solar metallicity stellar populations, in addition to allowing the user to vary the star formation history and the initial mass function. However, the derived evolutionary tracks are not fully self-consistent, since neither the stellar metallicity nor the IMF are permitted to vary as a function of time. For simplicity, a Salpeter (1955) IMF was adopted for all of the models considered here; a top- or bottom-heavy IMF will result in minor variations in the evolutionary tracks, but relative conclusions should be robust with regard to the choice of IMF. On the other hand, the lack of a self-consistent treatment of the chemical enrichment of subsequent stellar populations could have a severe impact on the derived star formation histories because of the well known age-metallicity degeneracy. Mono-metallicity models with similar star formation histories were used to explore the possible impact of the age-metallicity degeneracy on the derived stellar population ages (Figure 3). Each of the four panels in Figure 3 represent possible star formation histories; the first three are for exponentially decreasing star formation rates [ $\Psi(t) = \tau^{-1} \exp(-t/\tau)$ ; abbreviated as “tau models”, hereafter] and the last is for a constant star formation rate. In the small  $\tau$  models ( $\tau = 1$  or 5), the age-metallicity degeneracy is clearly evident in the overlapping age and metallicity contours for red systems. However, for blue objects (galaxies with  $B-V < 0.5$ ), the age-metallicity degeneracy is not as severe a problem; the metallicity induced variations in the evolutionary tracks primarily effect the U-B colors in these models, and have a small amplitude. Since the observed colors of the isolated dI sample are all quite blue ( $B-V < 0.5$ ), the derived composite stellar population models should provide reasonably accurate ages for the dominant stellar populations.

The derived galaxy evolution models included those for

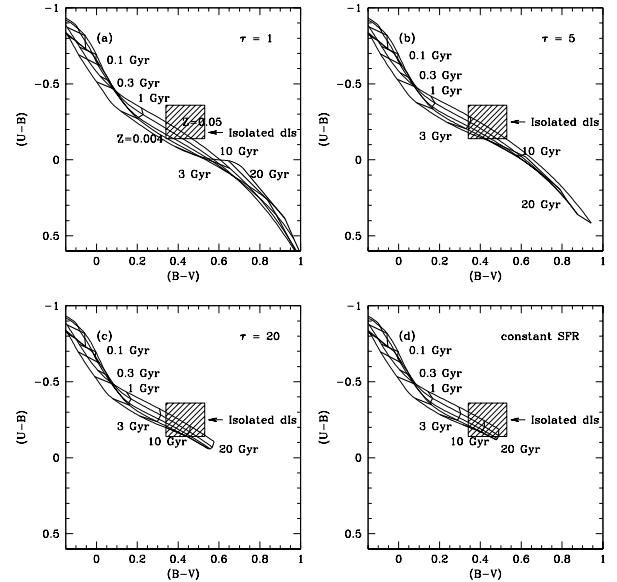


FIG. 3.— Color-color diagrams for mono-metallicity composite stellar populations from the Bruzual & Charlot (1996) stellar population models. Each panel represents a different star formation history, and shows the evolutionary tracks for different metallicities (1/5, 1/2.5, 1, and 2.5 times solar). The shaded box denotes the locus of colors for the majority of the galaxies in the isolated dI sample. (a) Predicted colors for  $\tau = 1$  Gyr models. The bold lines denote the locus for specific time steps; solid lines denote the evolutionary tracks for different metallicities. (b) Predicted colors for  $\tau = 5$  Gyr models. (c) Predicted colors for  $\tau = 20$  Gyr models. (d) Predicted colors for constant star formation rate models. In all of these models, the age-metallicity degeneracy is less significant for blue systems ( $B-V < 0.5$ ).

a single short starburst (10 Myr), a constant star formation rate, and several variations of exponentially decreasing star formation rates. At minimum, all star formation history models were run for both solar and 1/5 of solar metallicity, and many were run for all available metallicities (1/50 to 5 times solar). Examples of the color evolution of several of these models are shown in Figure 2; the color evolution tracks are marked every 0.5 dex, and time increases from the upper left hand corner to the lower right hand corner. For clarity, only the 1/5 of solar metallicity evolution tracks are shown (dwarf irregular galaxies typically have gas-phase abundances of 1/50 to 1/5 of solar, Skillman, Kennicutt, & Hodge 1989). Galaxies with short tau parameters, or galaxies which are dominated by a single burst of star formation, will have evolved into extremely red galaxies by the present epoch. In contrast, galaxies with long tau parameters ( $\tau \sim 10-20$  Gyr), or constant star formation rates, will still be blue systems, even after a Hubble time.

In addition to models with well defined star formation histories, several more complicated histories were also investigated. Figure 4 shows one such model, where a recent star burst has been superposed on top of a constant star formation rate. This particular model is for a starburst superposed on a galaxy which has had continuous star formation activity for 10 Gyr; the starburst consists of a brief period of time (500 Myr) where the star formation rate is 10 times the average past rate; after the starburst episode, the galaxy returns to its original star formation rate. As expected, the color evolution of the more complicated star

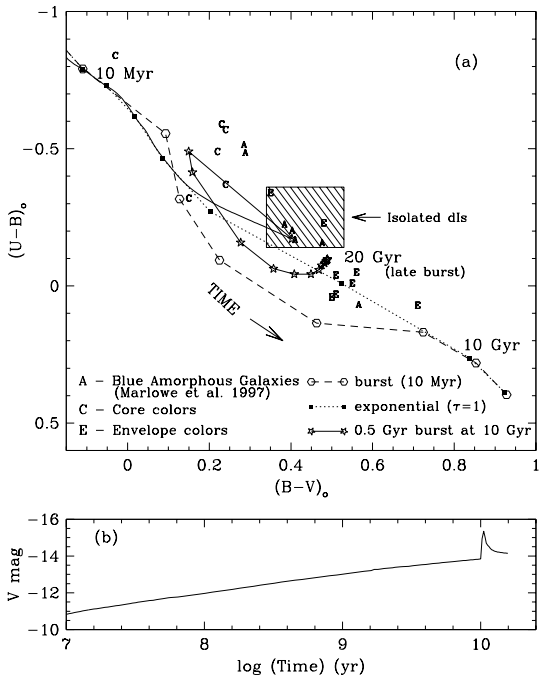


FIG. 4.— (a) Evolutionary tracks for low metallicity ( $1/5$  solar) composite stellar populations from the Bruzual & Charlot (1996) stellar population models. The short burst of star formation and exponentially decreasing star formation rate are the same as in Figure 2. Solid lines denote the color evolution of a system which undergoes a 0.5 Gyr burst of star formation (with  $\langle SFR \rangle_{\text{burst}} = 10 \times \langle SFR \rangle_{\text{past}}$ ) after having a quasi-continuous SFR for 10 Gyr. The stars mark time steps of 0.01 dex. Galaxies with  $B-V = 0.36$  and  $U-B = -0.06$  correspond to 750 Myr post-burst systems. The shaded box denotes the locus of colors for the majority of the galaxies in the isolated dI sample. In addition, colors of blue amorphous dwarf galaxies are shown (Marlowe et al. 1997;1999); the global colors of these starbursting systems are denoted by “A”, while the colors of the central core and extended stellar envelopes of the same galaxies are denoted by “C” and “E”, respectively. (b) Luminosity evolution for a system with a short burst of star formation at 10 Gyr superposed on a quasi-continuous star formation rate.

formation histories are a mixture of quiescent tracks and starburst tracks. For the brief period of time while a galaxy is undergoing a substantial starburst, both the  $B-V$  and  $U-B$  colors will be significantly affected by the young stellar population, and the observed colors will be bluer in  $U-B$  than expected for a simple composite stellar population. The extent to which this occurs depends on the burst strength (see, e.g., Huchra 1977; Larson & Tinsley 1978; Arimoto & Tarrab 1990; Krüger et al. 1991; van den Hoek et al. 2000). However, after the starburst fades, all models which combine a starburst superposed on a constant or decreasing star formation rate result in composite stellar populations which evolve through the locus of points between the short starburst (10 Myr, single population), and the exponentially decreasing star formation rate models (as illustrated in Figure 4). Thus, *the observed  $U-B$  color is an excellent tracer of previous starburst activity since any galaxy which has undergone a substantial starburst will be redder in  $U-B$  than expected for a simple composite stellar population.* Depending on the burst strength, these color offsets may exist for several Gyr, as the burst population evolves through the Red Giant Branch. In essence, the color offset from a nominal constant star formation rate evolutionary track is the result of the impact of the aging burst population on the luminosity

weighted colors. The  $U-B$  color is particularly sensitive to an aging burst population because it is dominated by the flux of the youngest, bluest stars; as these stars evolve, the  $U-B$  color changes rapidly, while the redder colors (i.e.,  $B-V$  and  $V-R$ ) change more slowly.

In the example shown here, a galaxy with  $B-V = 0.36$  and  $U-B = -0.06$  corresponds to a post-burst system where the last major episode of star formation occurred within the last 750 Myr. Of course, there are still ambiguities in the derived ages for galaxies in this region of the UBV color-color diagram since it is not immediately obvious if a galaxy is on a post-burst track (and, therefore, has an older underlying stellar population) or if a galaxy has an intrinsically short tau parameter. In other words, it is difficult to distinguish between an evolving post-burst population and a truly young galaxy based on optical colors alone. Nonetheless, these models suggest that galaxies which fill in this region of the UBV color-color diagram are likely to be post-burst systems whose age (time since most recent substantial star formation episode) can be approximated by the age of the corresponding stellar population from a short tau model.

The expected luminosity evolution of a galaxy which undergoes a brief starburst is shown in Figure 4b. The luminosity of the galaxy increases smoothly during the first 10 Gyr while the galaxy has a constant star formation rate; the starburst momentarily increases the luminosity by approximately 1.5 magnitudes; the integrated luminosity decreases immediately following the starburst as the dominant stellar population ages. Eventually, the newer stellar generations (formed at the lower rate) will again dominate the global colors (Figure 4a) and the integrated luminosity (Figure 4b). If the galaxy does not undergo additional starbursts, the net effect will be a slightly enhanced luminosity (relative to a constant star formation rate model) and  $U-B$  colors which are slightly redder than other galaxies with similar  $B-V$  colors.

### 3.3. Star Formation Histories from Global Colors

#### 3.3.1. The Isolated Dwarf Irregular Sample

Comparison of the observed colors with the galaxy evolution tracks indicates that the majority of the dwarf irregular galaxies appear to lie slightly above the constant star formation rate track (Figure 2). That is, the observed  $U-B$  color is slightly bluer than predicted by the composite stellar population models. Constant star formation rate models with higher metallicity stellar populations (solar metallicity and above) provide a slightly better fit than the lower metallicity models (see, e.g., Figure 3). However, it is unlikely that the stellar metallicities are solar or super-solar, given that the gas phase metallicities of these galaxies are quite low, typically  $\sim 1/10 - 1/5$  solar (van Zee & Haynes, in prep.). While this discrepancy is troubling, it is likely an artifact of the models, and in particular, may be due to the poorly understood physics of low metallicity massive stars (e.g., Lejeune et al. 1997). Given these problems, the uncertainties in the absolute stellar population ages are still quite large. Nonetheless, the observed colors for the majority of the isolated dwarf irregular galaxies appear to be most consistent with nearly constant star formation rates for at least 10 Gyr (Figure 2). That is, despite their blue colors, *dwarf irregular galaxies*

are not young systems.

The type of analysis presented here is similar to that presented in van Zee et al. (1997b) for LSB dwarf galaxies. The models used in van Zee et al. (1997b) were slightly older versions of the BC96 models, and the same offset existed between the observed and theoretical colors. In that paper, the observed colors were interpreted in the context of an aging stellar population, which indicated that the dominant stellar population in the LSB dwarf galaxies formed at least 1–3 Gyr ago. The optical colors of the LSB dwarf galaxies are actually quite similar to the global colors of the galaxies in the present sample, and thus, in retrospect, it is likely that the LSB dwarf galaxies also have had approximately constant star formation rates for roughly a Hubble time. Since the dominant stellar population in a system with continuous star formation activity will be *de facto* the most recently formed stars, i.e., those formed within the last few Gyr, this interpretation is consistent with that presented in van Zee et al. (1997b) for the LSB dwarf galaxies, but has additional implications about the age of the underlying stellar population.

Only the simplest star formation histories, systems where the star formation rate varies monotonically with time, are illustrated in Figure 2. However, it is also necessary to consider that the possibility that the isolated dwarf irregular galaxies have had a more episodic star formation history [as has been shown for nearby galaxies like the LMC (van den Bergh 1991; Girardi et al. 1995) and Carina (Smecker-Hane et al. 1994; Mighell 1997)]. An example of one of these more complicated star formation histories is illustrated in Figure 4a, where the locus of points for the dI sample are compared with the color evolution of a galaxy which undergoes a brief burst of star formation. From this representative model, it is clear that galaxies which are currently undergoing a starburst have colors which are too blue for the majority of the isolated dwarf galaxies, and post-starburst galaxies would be too red in  $U-B$  to fit the colors of the typical isolated dwarf irregular galaxy. Given that the current star formation rates of the isolated dwarf galaxies are quite low ( $\sim 0.02 M_{\odot} \text{ yr}^{-1}$ ) it is not too surprising that the starburst and post-starburst models do not apply to the majority of the galaxies in this sample.

There are a handful of galaxies which lie outside the locus shown in Figure 4a, however. UGC 9128, UGC 5205, and DDO 210 are all redder in  $U-B$  than expected for a constant star formation rate model, and all have extremely low or undetectable current star formation rates. Both UGC 9128 and DDO 210 have color gradients from the inner (blue) to the outer (red) regions. These galaxies may be examples of post-burst systems.

Two of these three galaxies have more detailed star formation histories derived from ground-based color-magnitude diagrams. DDO 210 is a nearby galaxy, and subtends a large angular size. Ground-based color-magnitude diagrams for DDO 210 indicate that it has had a recent enhancement of its star formation rate in the central regions within the last several Myrs (Lee et al. 1999), but its current star formation rate is negligible. Similarly, ground-based color-magnitude diagrams for the inner regions of UGC 9128 (DDO 187) indicate that its current star formation rate is  $\sim 3$  times smaller than its maximum

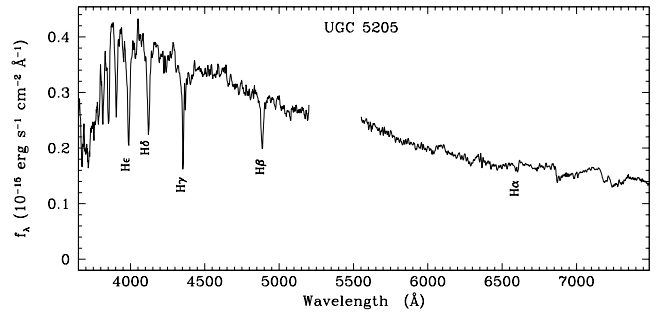


FIG. 5.— Optical spectrum of UGC 5205. The blue continuum level and presence of strong Balmer absorption features indicate that the last major episode of star formation occurred  $\sim 1$  Gyr ago in this system.

star formation rate which occurred a few tens of Myrs ago (Aparicio et al. 2000). Thus, both their global colors and detailed analysis of their stellar populations indicate that these galaxies are post-burst systems, in the sense that their current star formation rates are substantially lower than those of the recent past.

An accurate star formation history of the third galaxy with anomalous  $U-B$  colors, UGC 5205, has not yet been obtained, but additional insight into the star formation history of this galaxy can be gleaned from an optical spectrum of the inner region (Figure 5). While UGC 5205 has no detectable  $H\alpha$  emission in the narrow band image, the optical colors are still relatively blue; in addition, the inner region is knotty and irregular in appearance, suggesting recent star formation activity. The optical spectrum confirms that UGC 5205 is a post-burst galaxy. The strong Balmer absorption lines combined with the lack of Ca H and K and Mg Ib and the presence of a blue underlying continuum indicates that the stellar continuum is dominated by A-stars, exactly as expected for a post-burst system. Based on the integrated optical colors and optical spectrum, UGC 5205 appears to have had its last major star formation episode approximately 1 Gyr ago. UGC 5205 has a near neighbor (despite being included in an “isolated dwarf galaxy sample”), CGCG 007-025; the velocity difference between these two galaxies is  $84 \text{ km s}^{-1}$ , and the projected separation is approximately 8.3 kpc. Interestingly, the neighboring galaxy has a very high current star formation rate, and extremely blue colors (it has the bluest  $U-B$  of the entire sample). The dynamics of this pair are currently unconstrained, but the optical images reveal that UGC 5205 has a tidal tail, and thus has been disturbed by the interaction. In addition, the fact that the two galaxies are currently experiencing either an elevated (CGCG 007-025) or a quenched (UGC 5205) star formation rate suggests that their interaction has had a significant impact on the gas distribution and the star formation capability of the two systems.

In addition to UGC 9128, UGC 5205, and DDO 210, one other galaxy, UGC 12613, lies outside of the general locus of points for the isolated dwarf galaxy sample. UGC 12613 is the reddest galaxy in the sample in both  $U-B$  and  $B-V$ ; the optical colors are too red to be fit by a constant star formation rate model, but can be fit by either a declin-

ing star formation rate model (tau model), or by an aging burst population. The current star formation rate in UGC 12613 is extremely low, which supports the idea that UGC 12613 is dominated by an aging stellar population rather than by one which is constantly being replenished. However, there is one fundamental difference between UGC 12613 and the other three galaxies which may be post-burst galaxies: UGC 12613 is gas-poor. UGC 12613 has one of the lowest gas mass fractions (0.17) and one of the lowest values of  $M_{\text{HI}}/L_{\text{B}}$  (0.34) of all the galaxies in the sample. Thus, the current star formation rate may be low as a direct result of the fact that UGC 12613 is in the process of running out of fuel. The evolutionary tracks in Figure 4a indicate that if UGC 12613 is a post-burst galaxy, the last major star formation episode was several Gyr ago. This result is consistent with the more detailed stellar population models derived from observations of the resolved stellar population (Gallagher et al. 1998). Due to the small field of view of WFPC2, the HST observations only sampled the southwest quadrant of the galaxy (which includes the regions of current star formation activity). Gallagher et al. (1998) present several possible star formation histories for UGC 12613; their simplest model is that the star formation rate has been relatively constant for several Gyr, but that there was a recent episode of enhanced star formation activity which ended approximately 2 Gyr ago.

As demonstrated by these four unusual galaxies, the UBV color-color diagram can indeed identify systems with “bursty” star formation histories. The power of the star formation history analysis presented here lies in the fact that the majority of dwarf irregular galaxies lie within a small locus on the UBV color-color diagram: the “typical” dwarf irregular galaxy has had an approximately constant star formation rate, and galaxies which undergo a burst of star formation are the exception rather than the rule. This result agrees with the seminal work of Hunter & Gallagher (1985, 1986), based on the integrated colors of a diverse sample of dwarf and giant Irregular galaxies. In addition, the lack of significant color gradients in the “typical” dwarf irregular galaxies (Figure 1) implies that the entire stellar disk must have experienced a similar star formation history.

Inspection of the  $\text{H}\alpha$  images presented in Paper I (and those in e.g., Hunter et al. 1993; Miller & Hodge 1994; Miller 1996) indicate that the current star formation activity is distributed sparsely across the optical disk of each galaxy. Thus, while the optical colors indicate that the star formation activity is continuous, it is clear that the local star formation rate fluctuates, presumably as dense molecular clouds form and disperse. As first discussed by Hunter & Gallagher (1985), one way to reconcile the local and global star formation histories is to hypothesize that the star formation activity percolates across the entire stellar disk in a quasi-continuous manner. In other words, the global colors indicate a nearly constant star formation rate because they represent a temporal and spatial average of the composite stellar populations. In this model, the ensemble average of the star formation rate for the entire galaxy is approximately constant and every location in the disk has the potential to be a site for future star formation activity. Thus, in contrast to spiral galaxies where

the star formation occurs preferentially in the spiral arms and is presumably linked to the gas density enhancements from the spiral density waves, *star formation in dwarf irregular galaxies is a purely stochastic process, and has no favored location within the optical disk.*

### 3.3.2. Starbursting Dwarf Galaxies

Only three of the galaxies in the isolated dI sample were classified as starbursting dwarf galaxies: UGCA 439, UGC 11755, and CGCG 007-025 all have moderately high star formation rates, concentrated in the central regions of the galaxy. Of these three, only CGCG 007-025 stands out in the UBV color-color diagram as a galaxy with an unusual  $U-B$  color; UGC 11755 and UGCA 439 blend into the general trend. However, these three galaxies do stand out from the general sample in that their outer isophotes are significantly redder than their inner regions. Six other galaxies also had unusual color gradients from the inner to outer regions: UGC 685, UGC 1104, UGC 5288, UGC 9240, UGC 10351, and UGC 12713 (Figure 1). While these galaxies were not classified as Blue Compact Dwarfs (BCD), they all have unusually short scale lengths for their luminosities, and may be related to the BCD class. As with those galaxies classified as BCDs, the global colors of these 6 “compact dI’s” are not significantly different than those of a typical isolated dI.

This leads to the question of whether the UBV color-color diagram is sufficient to identify galaxies undergoing a current burst of star formation if only global colors are used. As mentioned in Section 3.1, the global color is a luminosity weighted color, and may not be representative of the composite stellar population if there are significant color gradients. The extent to which the optical colors are affected will depend not only on the strength and duration of the burst, but also on the spatial distribution of the young (bursting) stellar population: a centrally concentrated starburst will only affect the colors of the inner regions, and may not be sufficient to substantially change the global colors.

To investigate this further, the UBV colors for blue amorphous dwarf galaxies from Marlowe et al. (1997, 1999) are shown in Figure 4a. Like the starbursting dwarf galaxies in the isolated dI sample, all of the blue amorphous dwarf galaxies have a significant color gradient between their inner (starbursting) and outer regions. The location of the inner core region and outer envelopes are labelled as “C” (core) and “E” (envelope) in Figure 4a. As expected for galaxies with centrally concentrated starburst, the inner core regions are extremely blue while the outer envelope regions are much redder than the typical isolated dI. Clearly, the inner core regions of these galaxies are consistent with a starburst population superposed on an older (but still blue) stellar population, similar to the burst model shown here (also as discussed in detail by Marlowe et al. 1999). The red outer envelopes are consistent with aging stellar populations, i.e., ones in which the past star formation rate was higher than the present rate. The global colors are also shown in Figure 4a (labelled as “A” for average colors). Four of the starbursting dwarf galaxies have globally averaged colors which are typical of dI’s, and thus have similar properties to the three starbursting galaxies found in the isolated dI sample. The



fact that these galaxies have global colors which are consistent with quasi-continuous star formation activity indicates that the ensemble average of the inner (young) region and outer (old) region yields an intermediate age for the dominant stellar population, despite the current burst of star formation. Nonetheless, it is important to note that these galaxies are still easily separated from the “typical” dwarf irregular because of their strong color gradients. Of the remaining galaxies in the starbursting dwarf galaxy sample, two others (NGC 3125 and NGC 1705) have average colors which were similar to their inner core regions, indicating that the young stellar population is dominant, and one (NGC 3955) has a global color which is as red as the outer envelopes of the other galaxies, indicating that the central starburst is only a minor fraction of the total stellar population.

Based on this small sample of starbursting dwarf galaxies, it appears that a spatially resolved star formation history is extremely important in distinguishing between starbursting dwarf galaxies and “typical” dIs. Both types of galaxies may have similar global colors (depending on the relative strength of the star burst), but the star formation activity is centrally concentrated in the starbursting dwarf galaxies. Thus, the result of a starburst is to create a significant color gradient between the inner and outer regions of the optical disk.

#### 3.4. Other Constraints on the Star Formation History

The next question that needs to be addressed is whether a quasi-continuous star formation history is self-consistent with the observed luminosities and current star formation rates. There are two ways of looking at this question: (1) is the current star formation rate representative? and (2) can the galaxy continue to form stars at such a rate without running out of fuel in the near future? The first question addresses the issue of whether the star formation rate is approximately constant as a function of time while the second question addresses the issue of whether the fuel supply is sufficient to support the current star formation rate.

##### 3.4.1. Average Past Star Formation Rate

The average past star formation rate can be derived by estimating the total mass of stars formed and dividing this quantity by the length of time for which star formation has been taking place:

$$\langle SFR \rangle_{\text{past}} = \frac{M_{\text{stars}}}{T_{\text{sf}}}. \quad (2)$$

The latter quantity is relatively unconstrained, but, at maximum,  $T_{\text{sf}}$  must be less than the age of the universe. The total mass of stars formed is also uncertain, but can be estimated if one assumes a stellar mass-to-light ratio ( $\Gamma_b$ ) and estimates the amount of material that has been recycled during the history of the system ( $R$ ):

$$M_{\text{stars}} = \frac{\Gamma_b L_B}{(1 - R)}. \quad (3)$$

Kennicutt et al. (1994) investigated the average past star formation rates for a large sample of galaxies, spanning a range of Hubble types. They adopted a type-dependent mass-to-light ratio, a uniform recycling fraction of  $R =$

0.4, and a  $T_{\text{sf}}$  of 10 Gyr. They found that, on average, the earlier Hubble types had Scalo (1986)  $b$  parameters (ratio of current-to-past star formation rates) that were lower than later Hubble types, but that spiral galaxies generally had lower current star formation rates than their average past rate. This result is consistent with the idea that spiral galaxies have decreasing star formation rates, and that the observed color differences between the Hubble types may be a result of different star formation histories (e.g., Tinsley 1968; Searle et al. 1973).

Adopting a similar formalism, it is possible to derive the ratio of the current-to-past star formation rates for the isolated dwarf irregular galaxy sample. One of the difficulties for this type of analysis is that the stellar mass-to-light ratio is highly uncertain. The stellar mass-to-light ratios adopted by Kennicutt et al. (1994) were based on dynamical mass estimates, corrected for the contribution of dark matter; they adopted a V-band mass-to-light ratio of 0.6 for the irregular galaxies in their sample. However, the dynamical mass-to-light ratio is not well constrained for irregular galaxies; most dwarf irregular galaxies have solid body rotation throughout the optical disk (e.g., Skillman et al. 1987; Martimbeau, Carignan, & Roy 1994; van Zee et al. 1997c), and solid body rotation curves cannot be well fit by maximum disk models. In a similar analysis of the star formation history of dwarf galaxies, Miller & Hodge (1994) adopted a color dependent conversion formula for the mass-to-light ratio based on galaxy evolution models of Larson & Tinsley (1978). In their study, a typical dwarf galaxy ( $B - V = 0.4$ ) has a mass-to-light ratio of 1.0 in the B-band.

While it is somewhat circular reasoning to use a galaxy evolution code to derive a color dependent mass-to-light ratio in order to check the galaxy evolution model, at the very least such a model will provide a self-consistent estimate of the stellar mass. Thus, for consistency with the previous discussion, the mass-to-light ratio was derived using the BC96 code and a quasi-continuous star formation rate model:

$$\log \Gamma_b = 2.84(B - V) - 1.26 \quad (4)$$

where  $B - V$  is the observed color. This formalism results in a typical  $\Gamma_b$  of 0.8 for dwarf irregulars ( $B - V$  of 0.4), and is valid only for galaxies with  $B - V < 0.5$ .

The second necessary parameter for the derivation of the average past star formation rate is the recycling fraction, which is can be derived from the ratio between the total mass of stars formed over the history of the system and those still luminous at the present epoch. Using the BC96 code, the recycling fraction ( $R$ ) for a quasi-continuous star formation rate was found to be  $\sim 0.33$ ; that is, the total mass of stars formed is a factor of 1.5 times more than is presently detectable.

The final ingredient for this analysis is the age of the stellar population. Current estimates of the onset of star formation activity in the universe are on the order of  $z \sim 5 - 10$  (Steidel et al. 1999; Manning et al. 2000). Whether the galaxies in this sample began forming stars at this time is unknown, but it is not unreasonable to assume that they have been forming stars for approximately a Hubble time; thus, for  $H_0 = 75 \text{ km s}^{-1} \text{ Mpc}^{-1}$ ,  $T_{\text{sf}} \sim 13$  Gyr.

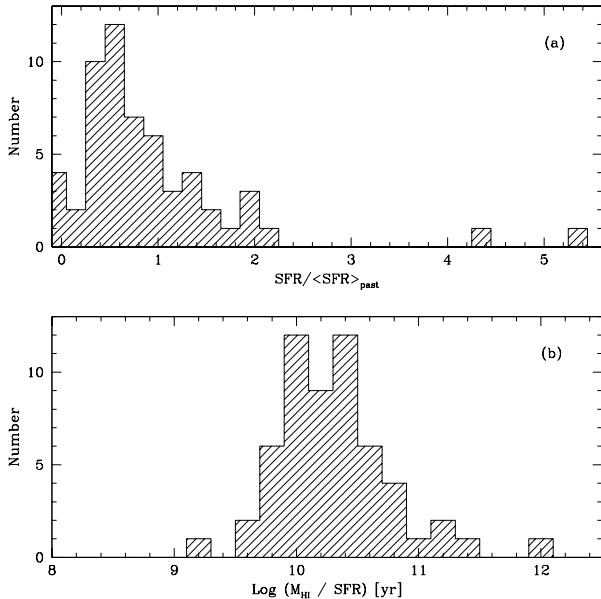


FIG. 6.— (a) The current star formation rate normalized by the average past star formation rate. For most of the dwarf irregular galaxies, the current star formation rate is approximately equal to the average past rate, supporting the idea that star formation is quasi-continuous. (b) The gas depletion time scales. Most of the dwarf irregular galaxies have long gas depletion time scales (on order of a Hubble time or more), and thus can continue to form stars at the present rate without running out of fuel.

The combination of higher mass-to-light ratios, a longer  $T_{\text{sf}}$ , and a slightly different current SFR conversion factor results in Scalo  $b$  parameters which are a factor of  $\sim 0.87$  times lower than the formalism for Irregular galaxies in Kennicutt et al. (1994). A histogram of  $b$  parameters derived from the above equations are shown in Figure 6a; the median value is  $0.7 \pm_{0.2}^{0.5}$ . For a quasi-continuous star formation rate, the current star formation rate should be similar to the average past rate. Thus, within the accuracy of this type of calculation, it appears that a quasi-continuous star formation rate is consistent with the observed integrated luminosities. Note that the extreme outliers ( $b > 2$ ) are the three star bursting galaxies in the sample, which have much higher current star formation rates than their average past rates.

In summary, both the optical colors and the integrated luminosities are well described by a constant star formation rate model. While it is important to remember that neither the luminosities nor the optical colors will be sensitive to a well evolved burst population (Figure 4), the fact that the current (low) star formation rates appear to be sufficient to build the observed stellar population over a Hubble time is compelling. If episodic bursts are the dominant mode of star formation, a larger fraction of the galaxies should be in a post-burst state, and there should be no correlation between the current star formation rate and the average past star formation rate. Thus, while it is impossible to completely rule out the possibility of early bursts of star formation, *the majority of galaxies in this sample do not need to have had substantial bursts at any epoch to build their present luminosity.* These simple arguments suggest that the dominant mode of star formation in dwarf irregular galaxies is one where star formation percolates slowly across the disk, with an nearly constant

average star formation rate.

### 3.4.2. Gas Depletion Timescales

Another important timescale argument concerns whether these galaxies can continue to sustain their current star formation activity for several more Gyr. The gas depletion time scale was calculated from the observed neutral hydrogen mass and current star formation rate:

$$\tau_g = \frac{M_{\text{HI}}}{\text{SFR}} \quad (5)$$

A histogram of the gas depletion time scales are shown in Figure 6b; the median gas depletion time scale is  $19 \pm_8^{14}$  Gyr. This clearly indicates that these galaxies are in no danger of running out of fuel, and can continue to form stars at the current star formation rate for at least another Hubble time.

It is important to note, however, that the quoted gas depletion timescales assume that the galaxy will be able to convert all of the available gas into stars. Spatially resolved maps of the neutral hydrogen distributions of dwarf galaxies indicate that a large fraction of the total hydrogen mass is located beyond the optical radius (e.g., Skillman et al. 1987, 1988; Carignan & Beaulieu 1989; Lo, Sargent, & Young 1993; Hoffman et al. 1996; van Zee et al. 1997c). It remains a mystery as to whether this extended gaseous material will be available for future star formation activity in these systems (see, e.g., Gallagher & Hunter 1984).

The simple lifetime arguments presented here indicate that the observed colors, luminosities, and gas properties are consistent with a quasi-continuous star formation rate. The fact that the isolated dwarf irregular galaxies have sufficient fuel to sustain similar star formation activity for at least another Hubble time provides additional support to the idea that star formation will continue to percolate (at a low rate) across the disks of these galaxies in a quasi-continuous manner for many Gyr to come.

### 3.5. Comparison to Resolved Stellar Population Models

As mentioned in the Introduction, the preferred method of determining the star formation history of a galaxy is to observe the resolved stellar population and count the relative number of stars in various evolutionary phases (main sequence, horizontal branch, blue loop, etc.). Color-magnitude diagrams (CMDs) provide a direct means of converting the number of stars at these evolutionary phases into a detailed star formation history. However, most galaxies are too distant to make such an analysis feasible. There are a few galaxies in the present sample which have been observed with HST, or are near enough that ground-based CMDs have been constructed, but these galaxies happen to be non-representative of the sample as a whole. The results of CMD analysis of UGC 9128, DDO 210, and UGC 12613 were presented in Section 3.3.1, where it was shown that all three of these galaxies are likely to be post-burst systems, in agreement with the observed optical colors. None of the other galaxies in the isolated dI sample have been observed with sufficient spatial resolution to derive detailed star formation histories, but it is nonetheless instructive to compare the results from integrated optical colors with the star formation histories derived from the resolved stellar populations of the nearest dwarf irregular galaxies.

Observations of the resolved stellar populations in starbursting dwarf galaxies indicate that star formation activity is both temporally and spatially confined. For example, the current star formation activity dominates the central regions of VII Zw 403 (UGC 6456), one of the nearest blue compact dwarf galaxies (Lynds et al. 1998). Analysis of the resolved stellar population indicates that the star formation rate peaked a few 100 Myr ago in VII Zw 403, and that the star formation activity is in a more quiescent stage at the present epoch (Lynds et al. 1998; Schulte–Ladbeck et al. 1999). At its peak, the star formation rate was  $\sim 30$  times higher than the typical star formation rate; this “burst” phase lasted for a few 100 Myr before returning a low level of star formation activity. Schulte–Ladbeck et al. (1999) emphasize that this was not the first episode of star formation in VII Zw 403, since intermediate–age and old metal–poor stars are distributed throughout the galaxy.

In sharp contrast with the starbursting dwarf galaxies, the “normal” dwarf irregular galaxies appear to have a more smoothly varying star formation history. Dohm–Palmer et al. (1998) summarized the results of HST observations of the resolved stellar populations of four Local Group dwarf galaxies: Sextans A, GR 8, UGC 12613 (Peg DIG), and Leo A. Not unexpectedly, each galaxy in this sample has a unique star formation history; however, certain commonalities exist. Of these four, only Sextans A appears to have had significant variations in the star formation activity over the last Gyr; however, unlike VII Zw 403, the current elevated star formation rate in Sextans A is only a factor of 3 higher than the past rate. In other words, none of these four galaxies appear to have undergone a significant starburst episode within the last Gyr. Thus, analysis of the resolved stellar populations provides additional confirmation that the star formation activity in most dwarf irregular galaxies occurs in a quasi–continuous manner, with a slow, but steady, conversion of gas into stars.

Finally, based on the spatial distribution of the resolved stellar population, Dohm–Palmer et al. (1998) found that star formation occurs at a low level across the entire stellar disk. In all four dI galaxies, the localized star forming complexes were found to occur on spatial scales similar to those of giant molecular clouds ( $\sim 100$  pc), and to last  $\sim 100$  Myr. At this time, only a few gas–rich dwarf galaxies have been observed with sufficient spatial resolution and depth to derive spatially resolved star formation histories. Clearly, further observations of the nearest gas–rich dwarf galaxies are needed to investigate the propagation of star formation activity in small galaxies. Of particular interest is the question of whether subsequent star formation activity is predominately a stochastic process, or if star formation propagates from one site to another in a more organized manner (as predicted by SSPSF).

#### 4. CURRENT STAR FORMATION ACTIVITY

As discussed in Section 3.4.1, the current star formation rate of the dI sample is approximately the same as the average past star formation rate. This implies that there is a correlation between current star formation rate and luminosity, since more luminous galaxies must have had a higher star formation rate in the past. It is thus necessary to normalize the current star formation rate by a scaling factor to remove obvious scaling correlations (i.e., big

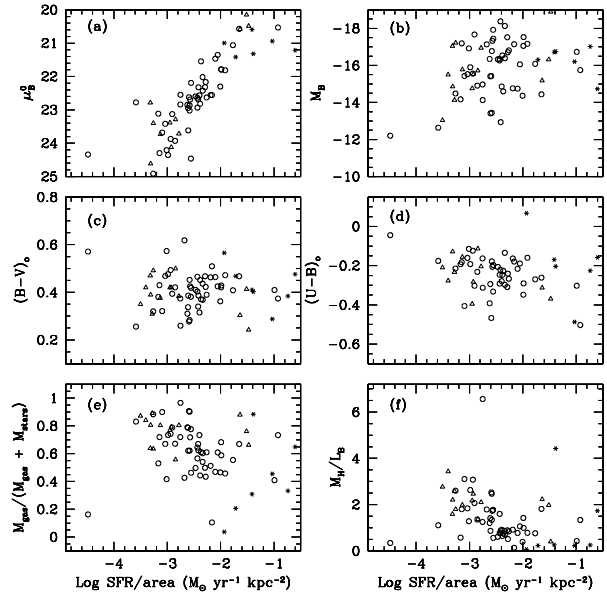


FIG. 7.— Correlations between the current star formation rate and other physical properties. Galaxies from the isolated dI sample are denoted by open circles; galaxies from van Zee et al. (1997) are denoted by open triangles; blue amorphous dwarf galaxies from Marlowe et al. (1997) are denoted by asterisks. The star formation rate has been normalized by the size of the galaxy, where  $\text{area} = 2\pi(1.5\alpha)^2$ . (a) A significant trend is evident in the relation between star formation rate per unit area and central surface brightness. Galaxies with low central surface brightness also have low normalized star formation rates. (b) No correlation is found between absolute magnitude and the normalized star formation rate. (c) No correlation is found between normalized star formation rate and  $B-V$  or (d)  $U-B$ . (e) Correlation between gas mass fraction (baryonic) and star formation rate. In this sample, galaxies which are currently gas–rich also have low normalized star formation rates, although the converse does not hold. (f) A weak correlation is seen between gas–richness, as measured by  $M_H/L_B$ , and star formation rate per unit area.

galaxies are big). One way to normalize the current star formation rate is to divide by the surface area of the galaxy (e.g., Hunter & Gallagher 1986). In the following analysis, “area” has been defined in terms of scale length:  $r=1.5\alpha$ . The choice of  $1.5\alpha$  is arbitrary, but it roughly corresponds to  $R_{26.5}$  for this sample. The normalized current star formation rate is plotted against a variety of physical parameters in Figure 7; these plots include galaxies from both the present sample, the LSB dwarf galaxies from van Zee et al. (1997b), and the blue amorphous dwarf galaxies from Marlowe et al. (1997). The use of a normalized star formation rate removes the correlation between star formation activity and luminosity (Figure 7b) but introduces a correlation between surface brightness and normalized star formation rate (Figure 7a). However, this is exactly the correlation one would expect for galaxies with quasi–continuous star formation: high surface brightness galaxies must have had high star formation rates per unit area (see also Hunter 1997). Thus, in the subsequent plots one can consider either surface brightness or normalized star formation rate as the ordinate on the abscissa.

Figure 7(c,d) shows that there is no correlation between normalized star formation rate and the optical colors. That is, the normalized star formation rate (and, consequently, the surface brightness) is independent of the exact star formation history. This lack of correlation be-

tween age and surface brightness is also seen in large LSB disk galaxies (e.g., O’Neil et al. 1997; Bell et al. 1999; Knezek 1999). Thus, the central surface brightness of a galaxy appears to be an intrinsic property, not a result of differing evolutionary stages.

The final two plots in Figure 7 investigate the relationship between current star formation activity and gas properties of dwarf galaxies. The gas properties are particularly relevant because the gas provides fuel for star formation activity. In many ways, the gas–richness of a galaxy is a good indicator of evolutionary status, insofar as a gas–rich galaxy has not converted much of its gas into stars. Note, however, that this does not necessarily imply that a gas–rich galaxy is “young,” since a galaxy with a low star formation rate will take longer to convert gas into stars.

Figure 7e shows a weak trend of normalized star formation rate with gas mass fraction. The gas mass fraction is the ratio of the total gas mass ( $M_{\text{gas}}$ ) to the total baryonic mass ( $M_{\text{gas}} + M_{\text{stars}}$ ). The stellar mass was computed as described in Section 3.4.1 and the gas mass includes a correction for the neutral helium component [ $M_{\text{gas}} = 1.3 \times M_{\text{HI}}$ , (Anders & Grevesse 1989)]. The molecular gas component is neglected for this computation since it is difficult to detect CO in low mass galaxies (e.g., Elmegreen, Elmegreen, & Morris 1980; Taylor, Koblunicky, & Skillman 1998), and, further, the correction from CO to H<sub>2</sub> column density is highly uncertain for low metallicity galaxies (e.g., Verter & Hodge 1995; Wilson 1995). For a simple model of galaxy evolution, the gas mass fraction is initially unity (pure gas disk) and then decreases as the gas is converted into stars. The correlation seen in Figure 7e indicates that higher surface brightness galaxies (high normalized star formation rate galaxies) have lower gas mass fractions. This is exactly the trend expected if the average past star formation rate is similar to the present rate: galaxies with high star formation rates will convert a larger fraction of their gas into stars by the present epoch, and therefore have both higher surface brightness and lower gas mass fractions. This trend is also seen in samples of disk galaxies (McGaugh & de Blok 1997). However, there are a few galaxies which counter this trend, such as UGC 12613. UGC 12613 has both a low normalized star formation rate and a low gas mass fraction. In fact, dwarf transition galaxies (e.g., Knezek, Sembach, & Gallagher 1999) and gas–poor ellipticals, such as NGC 205 (Young & Lo 1997), should fill in the lower left region of the diagram. The upper right, however, is likely to be genuinely devoid of galaxies at the present epoch since a high normalized star formation rate will rapidly process the gas, and thus a galaxy should evolve quickly from this region.

A similarly weak trend is seen in the plot of  $M_{\text{HI}}/L_B$  (Figure 7f). The galaxies in this sample span only a small range in  $M_{\text{HI}}/L_B$ , but the gas–rich systems again appear to be the systems with lower normalized star formation rates (again with the exception of UGC 12613). However, it is also important to note that not all low surface brightness galaxies are unusually gas–rich, and, conversely, not all gas–rich galaxies have extremely low surface brightness (e.g., DDO 154, Carignan & Beaulieu 1989).

The majority of the galaxies in the present sample are gas–rich systems, with gas mass fractions greater than 0.4 (Figure 7e). However, if these galaxies have an abundant

supply of gas, why haven’t they converted it into stars in an efficient manner? In fact, one of the puzzling results of studies of the gas distribution in dwarf galaxies is that both extreme LSB and “normal” dwarf irregular galaxies have gas densities which are well below the threshold for star formation activity, despite the fact that these galaxies are considered gas–rich systems (e.g. Hunter & Plummer 1996; van Zee et al. 1997c; Hunter, Elmegreen & Baker 1998). This result may hold the key to explaining both why these galaxies are still gas–rich and why the star formation activity is quasi–continuous in normal dwarf irregular galaxies: the gas disk is globally stable against gravitational collapse. If this is correct, star formation can occur only in localized regions of enhanced gas density. Further, since the likelihood is small that any region will increase its density enough to exceed the threshold density, star formation activity will occur at a very low rate across the stellar disk. Combined with the fact that the gas density is almost constant throughout the optical extent, this suggests that star formation activity percolates randomly across the entire stellar disk in an inefficient manner, thereby creating a dominant young stellar population at all locations while retaining a high gas mass fraction.

## 5. CONCLUSIONS

Optical colors and global star formation rates for a sample of isolated dwarf irregular galaxies have been interpreted in the context of composite stellar population models. The major results are summarized below.

(1) The majority of dwarf irregular galaxies have minor or non–existent color gradients across their stellar disks, and thus global colors accurately reflect the evolutionary status of the entire stellar component. The few galaxies in this sample which do have significant color gradients have very short scale lengths for their luminosities, and may be related to the class of starbursting dwarf galaxies.

(2) The global colors are blue, with median values of  $B-V = 0.42 \pm_{0.05}^{0.04}$  and  $U-B = -0.22 \pm_{0.07}^{0.04}$ . The observed luminosities, optical colors, and current star formation rates are consistent with an approximately constant integrated star formation rate over the age of the universe (see also Hunter & Gallagher 1985). In addition, typical gas depletion timescales are  $\sim 20$  Gyr, indicating that these galaxies can continue to form stars at the present rate for at least another Hubble time.

(3) There is no correlation between surface brightness and star formation history. The only significant correlation in physical parameters is that low surface brightness galaxies have low normalized star formation rates (see also Hunter & Gallagher 1986). Weak trends suggest that most low surface brightness galaxies are also gas–rich, as traced by gas mass fraction and  $M_{\text{HI}}/L_B$ .

At the very minimum, galaxy evolution models must be able to reproduce the global properties of a galaxy such as colors, luminosity, current star formation rate, gas mass fraction, and metallicity. As shown throughout this paper, the observed global properties of the typical dwarf irregular galaxy are well fit by a constant average star formation rate, with a typical age of  $\sim 10$  Gyr. Combined with the studies of the resolved stellar populations of dwarf galaxies in the Local Group (e.g., Dohm–Palmer et al. 1998), this argues against the possibility that most dwarf irregular

galaxies have a significant starburst phase. Rather, star formation percolates throughout the stellar disk at a slow, but approximately constant, rate. Thus, while starburst models are necessary to explain the observed properties of a few dwarf galaxies, these galaxies are the exception, not the rule.

If this interpretation is correct, then the majority of dwarf irregular galaxies in the local universe are unlikely to be the evolutionary remnants of the “faint blue galaxies” found at intermediate redshift (e.g., Cowie, Songaila, & Hu 1991; Driver, Windhorst, & Griffiths 1995). Several models have shown that it is possible to reproduce the excess of faint blue galaxies found in deep surveys by including a rapidly evolving population of low luminosity galaxies whose star formation rates peak at  $z \sim 1$  (e.g., Babul & Rees 1992; Babul & Ferguson 1996). The basic reasoning of these models is that the luminosity of a starbursting dwarf galaxy may be sufficiently elevated to allow it to be included in a deep survey, but its evolutionary remnant will be too faint to be included in surveys of the local galaxy population. Thus, the difference in the derived local and intermediate- $z$  luminosity functions creates an “excess” of faint blue galaxies at intermediate- $z$ . However, these models require that formation of dwarf galaxies be delayed until  $z \sim 1$  so that the star formation rates peak at the appropriate epoch. This does not appear to be the case for the typical dwarf irregular, and thus the dwarf irregular class probably does not contribute significantly to the excess population of faint blue galaxies. Of course, these models do not rule out the possibility that the faint blue galaxies are related to gas-poor objects at the present epoch, such as dwarf elliptical galaxies.

Finally, the star formation history of the typical dwarf irregular galaxy is substantially different than that of a

massive spiral or elliptical galaxy. Standard stellar population models for spiral galaxies indicate that the observed colors are best fit by declining star formation rates (e.g., Larson & Tinsley 1978) while the colors of elliptical galaxies are best fit by evolving stellar populations (e.g., Worthey 1994). Schematically, the star formation history of the universe is also in agreement with these stellar population models; the most recent models indicate that the star formation rate of the universe was substantially higher in the past than it is today (e.g., Pei & Fall 1995; Lilly et al. 1995; Madau et al. 1996). In contrast, dwarf irregular galaxies appear to be forming stars at approximately the same low rate now as they were several Gyr ago. Further, since dwarf galaxies are still extremely gas-rich systems, they can continue to convert gas into stars at the same low rate for many Gyr to come. Thus, at some point in the future, dwarf irregular galaxies may be the only systems which will retain sufficient fuel to continue forming stars; in other words, it is only a matter of time before dwarf galaxies dominate the star formation activity of the universe.

Elizabeth Barton, David Schade, and Bev Oke are gratefully acknowledged for numerous thought-provoking conversations about galaxy formation and evolution. Stéphanie Côté and Vicki Weafer provided helpful comments on early versions of this paper. Martha Haynes kindly provided access to the Palomar 5m telescope for the spectroscopic observations of UGC 5205. This research has made use of the NASA/IPAC Extragalactic Database (NED) which is operated by the Jet Propulsion Laboratory, California Institute of Technology, under contract with the National Aeronautics and Space Administration.

## REFERENCES

- Almoznino, E., & Brosch, N. 1998, *MNRAS*, 298, 931  
 Anders, E., & Grevesse, N. 1989, *Geochim. Cosmochim. Acta*, 53, 197  
 Aparicio, A., Tikhonov, N., & Karachentsev, I. 2000, *AJ*, 119, 177  
 Arimoto, N., & Tarrab, I. 1990, *A&A*, 228, 6  
 Babul, A., & Rees, M. J. 1992, *MNRAS*, 255, 346  
 Babul, A., & Ferguson, H. C. 1996, *ApJ*, 458, 100  
 Bell, E. F., Bower, R. G., de Jong, R. S., Hereld, M., L., & Raucsher, B. J. 1999, *MNRAS*, 302, 55  
 Bruzual A., G., & Charlot, S. 1993, *ApJ*, 405, 538  
 Bruzual A., G., & Charlot, S. 1996, in prep. (BC96)  
 Carignan, C., & Beaulieu, S. 1989, *ApJ*, 347, 760  
 Cowie, L. L., Songaila, A., & Hu, E. M. 1991, *Nature*, 354, 460  
 de Vaucouleurs, G., de Vaucouleurs, A., Corwin, H. G., Buta, R., Paturel, G., & Fouqué, P. 1991, *Third Reference Catalogue of Bright Galaxies* (Springer, New York) (RC3)  
 Dohm-Palmer, R. C., Skillman, E. D., Gallagher, J., Tolstoy, E., Mateo, M., Dufour, R. J., Saha, A., Hoessel, J., & Chiosi, C. 1998, *AJ*, 116, 1227  
 Dohm-Palmer, R. C., Skillman, E. D., Saha, A., Tolstoy, E., Mateo, M., Gallagher, J., Hoessel, J., Chiosi, C., & Dufour, R. J. 1997, *AJ*, 114, 2527  
 Doublier, V., Caulet, A., & Comte, G. 1999, *A&AS*, 138, 213  
 Doublier, V., Comte, G., Petrosian, A., Surace, C., & Turatto, M. 1997, *A&AS*, 124, 405  
 Driver, S. P., Windhorst, R. A., & Griffiths, R. E. 1995, *ApJ*, 453, 48  
 Elmegreen, B. G., Elmegreen, D. M., & Morris, M. 1980, *ApJ*, 240, 455  
 Fisher, J.R., & Tully, R.B., 1981, *ApJS*, 47, 139  
 Gallagher, J. S., & Hunter, D. A. 1984, *ARA&A*, 22, 37  
 Gallagher, J. S., Hunter, D. A., & Tutukov, A. V. 1984, *ApJ*, 284, 544  
 Gallagher, J. S., Tolstoy, E., Dohm-Palmer, R. C., Skillman, E. D., Cole, A. A., Hoessel, J. G., Saha, A., & Mateo, M. 1998, *AJ*, 115, 1869  
 Girardi, L. et al. 1995, *A&A*, 298, 87  
 Gerola, H., Seiden, P. E., & Schulman, L. S. 1980, *ApJ*, 242, 517  
 Giovanelli, R., Avera, E., & Karachentsev, I. D. 1997, *AJ*, 114, 122  
 Giovanelli, R., & Haynes, M. P. 1993, *AJ*, 105, 1271  
 Greggio, L., Marconi, G., Tosi, M., & Focardi, P. 1993, *AJ*, 105, 894  
 Greggio, L., Tosi, M., Clampin, M., De Marchi, G., Leitherer, C., Nota, A., & Sirianni, M. 1998, *ApJ*, 504, 725  
 Hardy, E. 1978, *PASP*, 90, 132  
 Haynes, M. P., Hogg, D. E., Maddalena, R. J., Roberts, M. S., & van Zee, L. 1998, *AJ*, 115, 62  
 Heller, A., Almoznino, E., & Brosch, N. 1999, *MNRAS*, 304, 8  
 Hoffman, G. L., Salpeter, E. E., Farhat, B., Roos, T., Williams, H., & Helou, G. 1996, *ApJS*, 105, 269  
 Holtzman, J. A. et al. 1999, *AJ*, 118, 2262  
 Hopp, U. 1999, *A&AS*, 134, 317  
 Huchra, J. P. 1977, *ApJ*, 217, 928  
 Hunter, D. A. 1997, *PASP*, 109, 937  
 Hunter, D. A., Elmegreen, B. G., & Baker, A. L. 1998, *ApJ*, 493, 595  
 Hunter, D. A. & Gallagher, J. S., 1985, *ApJS*, 58, 533  
 Hunter, D. A. & Gallagher, J. S., 1986, *PASP*, 98, 5  
 Hunter, D. A., Hawley, W. N., & Gallagher, J. S. 1993, *AJ*, 106, 1797  
 Hunter, D. A., & Plummer, J. D. 1996, *ApJ*, 462, 732  
 Hunter, D. A., & Thronson, H. A. 1995, *ApJ*, 452, 238  
 Kennicutt, R. C. 1998, *ARA&A*, 36, 189  
 Kennicutt, R. C., Tamblyn, P., & Congdon, C. W. 1994, *ApJ*, 435, 22  
 Knezek, P. 1999, in ‘The Low Surface Brightness Universe’, *ASP Conf. Series* 170, ed. J. I. Davies, C. Impey, & S. Phillipps, (San Francisco: ASP) p. 191  
 Knezek, P., M., Sembach, K. R., & Gallagher, J. S. 1999, *ApJ*, 514, 119

- Krüger, H., Fritze-van Alvensleben, U., Loose, H.-H., & Fricke, K. J. 1991, *A&A*, 242, 343
- Larson, R. B., & Tinsley, B. M. 1978, *ApJ*, 219, 46
- Lee, M. G., Aparicio, A., Tikhonov, N., Byun, Y.-I., & Kim, E. 1999, *AJ*, 118, 853
- Leitherer et al. 1996, *PASP*, 108, 996
- Lejeune, Th., Cuisinier, F., & Buser, R. 1997, *A&AS*, 125, 229
- Lilly, S. J., Tresse, L., Hammer, F., Crampton, D., & Le Fèvre, O. 1995, *ApJ*, 455, 108
- Lo, K. Y., Sargent, W. L. W., & Young, K. 1993, *AJ*, 106, 507
- Lynds, R., Tolstoy, E., O'Neil, E. J., & Hunter, D. A. 1998, *AJ*, 116, 146
- Madau, P., Ferguson, H. C., Dickinson, M. E., Giavalisco, M., Steidel, C. C., & Fruchter, A. 1996, *MNRAS*, 283, 1388
- Makarova, L., Karachentsev, I., Takalo, L. O., Heinämäki, P., & Valtonen, M. 1998, *A&AS*, 128, 459
- Manning, C., Stern, D., Spinrad, H., & Bunker, A. J. 2000, *ApJ*, 537, 65
- Marconi, G., Tosi, M., Greggio, L., & Focardi, P. 1995, *AJ*, 109, 173
- Marlowe, A. T., Meurer, G. R., & Heckman, T. M. 1999, *ApJ*, 522, 183
- Marlowe, A. T., Meurer, G. R., Heckman, T. M., & Schommer, R. 1997, *ApJS*, 112, 285
- Martimbeau, N., Carignan, C., & Roy, J.-R. 1994, *AJ*, 107, 543
- Massey, P., Strobbe, K., Barnes, J. V., & Anderson, E. 1988, *ApJ*, 328, 315
- McGaugh, S. S., & de Blok, W. J. G. 1997, *ApJ*, 481, 689
- Mighell, K. J. 1997, *AJ*, 114, 1458
- Miller, B. W. 1996, *AJ*, 112, 991
- Miller, B. W., & Hodge, P. 1994, *ApJ*, 427, 656
- Nilson, P., 1973, *Uppsala General Catalog of Galaxies (Uppsala) (UGC)*
- O'Neil, K., Bothun, G. D., Schombert, J. M., Cornell, M. E., & Impey, C. D. 1997, *AJ*, 114, 2448
- Papaderos, P., Loose, H.-H., Thuan, T. X., & Fricke, K. J. 1996, *A&AS*, 120, 207
- Pei, Y. C., & Fall, S. M. 1995, *ApJ*, 454, 69
- Roye, E. W., & Hunter, D. A. 2000, *AJ*, 119, 1145
- Salpeter, E. E. 1955, *ApJ*, 121, 161
- Salzer, J. J., di Serego Alighieri, S., Matteucci, F., Giovanelli, R., & Haynes, M. P. 1991, *AJ*, 101, 1258
- Scalo, J. M. 1986, *Fund. Cosmic Physics*, 11, 1
- Schechter, P. 1980, *AJ*, 85, 801
- Schlegel, D. J., Finkbeiner, D. P., & Davis, M. 1998, *ApJ*, 500, 525
- Schneider, S. E., Thuan, T. X., Magri, C., & Wadiak, J. E. 1990, *ApJS*, 72, 245
- Schneider, S. E., Thuan, T. X., Mangum, J. G., & Miller, J. 1992, *ApJS*, 81, 5
- Schulte-Ladbeck, R. E., Hopp, U., Crone, M. M., & Greggio, L. 1999, *ApJ*, 525, 709
- Searle, L., & Sargent, W. L. W. 1972, *ApJ*, 173, 25
- Searle, L., Sargent, W. L. W., & Bagnuolo, W. G. 1973, *ApJ*, 179, 427
- Skillman, E. D., Bothun, G. D., Murray, M. A., & Warmels, R. H. 1987, *A&A*, 185, 61
- Skillman, E. D., Kennicutt, R. C., & Hodge, P. W. 1989, *ApJ*, 347, 875
- Skillman, E. D., Terlevich, R. J., Teuben, P. J., & van Woerden, H. 1988, *A&A*, 198, 33
- Smecker-Hane, T. A., Stetson, P. B., Hesser, J. E., & Lehnert, M. D. 1994, *AJ*, 108, 507
- Steidel, C. C., Adelberger, K. L., Giavalisco, M., Dickinson, M., & Pettini, M. 1999, *ApJ*, 519, 1
- Strobel, N. V., Hodge, P., & Kennicutt, R. C. 1991, *ApJ*, 383, 148
- Taylor, C. L., Kobulnicky, H. A., & Skillman, E. D. 1998, *AJ*, 116, 2746
- Tifft, W. G., & Cocke, W. J. 1988, *ApJS*, 67, 1
- Tinsley, B. M. 1968, *ApJ*, 151, 547
- Tinsley, B. M. 1980, *Fund. Cosmic Physics*, 5, 287
- Tolstoy, E. 1996, *ApJ*, 462, 684
- Tolstoy, E., Gallagher, J. S., Cole, A. A., Hoessel, J. G., Saha, A., Dohm-Palmer, R. C., Skillman, E. D., Mateo, M., Hurley-Keller, D. 1998, *AJ*, 116, 1244
- Tosi, M., Greggio, L., Marconi, G., & Focardi, P. 1991, *AJ*, 102, 951
- van den Bergh, S. 1991, *ApJ*, 369, 1
- van den Hoek, L. B., de Blok, W. J. G., van der Hulst, J. M., & de Jong, T. 2000, *A&A*, 357, 397
- van Zee, L. 2000, *AJ*, 119, 2757 (Paper I)
- van Zee, L., & Haynes, M. P., in prep.
- van Zee, L., Haynes, M. P., & Salzer, J. J. 1997a, *AJ*, 114, 2497
- van Zee, L., Haynes, M. P., Salzer, J. J., & Broeils, A. H. 1997b, *AJ*, 113, 1618
- van Zee, L., Maddalena, R. J., Haynes, M. P., Hogg, D. E., & Roberts, M. S. 1997c, *AJ*, 113, 1638
- van Zee, L., Salzer, J. J., Haynes, M. P., O'Donoghue, A. A., & Balonek, T. J. 1998, *AJ*, 116, 2805
- Verter, F., & Hodge, P. W. 1995, *ApJ*, 446, 616
- Wilson, C. D. 1995, *ApJ*, 448, L97
- Worthey, G. 1994, *ApJS*, 95, 107
- Young, L. M., & Lo, K. Y. 1997, *ApJ*, 476, 127

Table 1. Observed Properties of the Isolated Dwarf Galaxy Sample

UGC Number	Alternate Name	Morph. Type	$i$ (deg)	$m_B$	(B-V) <sub>0</sub>	(U-B) <sub>0</sub>	$\int S dv$ (Jy km s <sup>-1</sup> )	Vel. (km s <sup>-1</sup> )	W <sub>20</sub> (km s <sup>-1</sup> )	M <sub>H</sub> /L <sub>B</sub> (M <sub>⊙</sub> /L <sub>⊙</sub> )	notes
Primary Sample											
UGC 191	DDO 2	Sm	42	13.71 ± 0.07	0.46 ± 0.03	-0.31 ± 0.05	19.34	1143	139	0.9	a
UGC 231	NGC 100	Sc	89	13.57 ± 0.05	0.61 ± 0.02	...	44.30	842	222	1.8	b
UGC 290		Sdm	83	16.04 ± 0.13	0.31 ± 0.05	-0.21 ± 0.09	6.61	767	98	2.6	c
UGCA 9	DDO 226	IB(s)m	64	14.42 ± 0.08	0.38 ± 0.04	-0.19 ± 0.07	6.50	361	81	0.6	d
UGCA 15	DDO 6	IB(s)m	65	15.30 ± 0.11	0.30 ± 0.06	-0.22 ± 0.11	4.48	303	47	0.9	d
UGC 634	DDO 7	SABm	60	14.81 ± 0.08	0.39 ± 0.03	-0.30 ± 0.06	16.21	2211	161	2.1	a
UGC 685		SAm	45	13.96 ± 0.08	0.46 ± 0.02	-0.22 ± 0.04	13.38	156	96	0.8	e
UGC 891	DDO 10	SABm	71	14.58 ± 0.04	0.46 ± 0.03	-0.16 ± 0.06	17.82	643	144	1.8	b
UGC 1104		Im	63	14.14 ± 0.03	0.40 ± 0.01	-0.27 ± 0.02	11.07	681	123	0.8	f
UGC 1175		Sm:	38	16.14 ± 0.08	0.26 ± 0.04	-0.31 ± 0.06	15.14	728	106	6.6	a
UGC 1281		Sdm	84	13.40 ± 0.04	0.42 ± 0.03	-0.23 ± 0.04	39.20	156	136	1.4	g
UGC 1501	NGC 784	SBdm: sp	75	12.15 ± 0.05	0.40 ± 0.03	-0.25 ± 0.04	70.00	199	124	0.8	g
UGC 2023	DDO 25	Im:	26	13.50 ± 0.12	0.44 ± 0.04	-0.25 ± 0.07	17.00	603	54	0.6	g
UGC 2345	DDO 30	SB(rs)m:	31	14.21 ± 0.14	0.42 ± 0.06	-0.20 ± 0.09	23.62	1508	116	1.7	d
UGC 2603	Mailyan 2	Im	61	14.43 ± 0.09	0.31 ± 0.08	-0.22 ± 0.22	8.82	2516	162	0.8	f
UGCA 61		SB(s)m: sp	82	13.78 ± 0.08	0.38 ± 0.04	-0.33 ± 0.08	36.14	1735	182	1.8	d
UGC 3371	DDO 39	Im:	55	13.71 ± 0.19	0.56 ± 0.07	-0.11 ± 0.17	27.66	820	149	1.3	d
UGC 3647	DDO 40	IBm	32	14.41 ± 0.06	0.42 ± 0.03	-0.35 ± 0.05	16.16	1386	83	1.4	b
UGC 3672		Im	56	15.09 ± 0.17	0.27 ± 0.05	-0.47 ± 0.06	15.43	979	131	2.5	a
UGC 4117		IBm	64	15.15 ± 0.05	0.31 ± 0.02	-0.28 ± 0.04	5.29	775	80	0.9	h
UGC 4121	DDO 48	Sm:	80	15.08 ± 0.09	0.47 ± 0.06	-0.19 ± 0.08	16.09	1090	165	2.6	d
UGC 4325	NGC 2552	SA(s)m?	49	12.71 ± 0.04	0.42 ± 0.03	-0.24 ± 0.03	27.87	524	156	0.5	b
UGC 5205		SBm pec?	52	14.96 ± 0.07	0.31 ± 0.02	-0.08 ± 0.04	8.07	1536	68	1.2	i
CGCG 007-025											
		Sm	39	15.50 ± 0.05	0.37 ± 0.02	-0.50 ± 0.10	5.57	1452	126	1.3	i
UGC 5288		Sdm:	35	14.18 ± 0.08	0.46 ± 0.06	-0.26 ± 0.06	25.59	561	116	1.8	d
UGC 5414	NGC 3104	IAB(s)m	54	13.19 ± 0.04	0.37 ± 0.03	-0.30 ± 0.04	25.01	603	134	0.7	b
UGC 9128	DDO 187	ImIV-V	49	14.36 ± 0.06	0.25 ± 0.05	-0.18 ± 0.04	13.27	153	52	1.1	a
UGC 9211	DDO 189	Im:	45	14.76 ± 0.09	0.32 ± 0.07	-0.40 ± 0.11	25.53	686	123	3.1	b
UGC 9219	NGC 5608	Im:	64	13.76 ± 0.04	0.41 ± 0.03	-0.21 ± 0.04	12.67	662	159	0.6	d
UGC 9240	DDO 190	IAm	28	13.27 ± 0.04	0.37 ± 0.03	-0.23 ± 0.04	24.39	150	85	0.7	b
UGC 9500	DDO 196	Sm:	21	15.00 ± 0.17	0.45 ± 0.05	-0.18 ± 0.09	8.85	1690	37	1.3	d
UGC 9992		Im	52	14.70 ± 0.10	0.37 ± 0.04	-0.16 ± 0.05	10.86	429	52	1.2	d
UGC 10054	DDO 203	SBdm	61	13.68 ± 0.04	0.43 ± 0.04	-0.13 ± 0.06	19.30	1496	210	0.9	f
UGC 10310	DDO 204	SB(s)m	31	13.62 ± 0.06	0.39 ± 0.05	-0.27 ± 0.08	19.79	716	108	0.8	b
UGC 10351		Sdm:	57	14.68 ± 0.05	0.42 ± 0.03	-0.19 ± 0.04	9.45	891	77	1.1	f
UGC 10445	VV 625	SBc	33	13.36 ± 0.05	0.42 ± 0.03	-0.29 ± 0.04	29.68	963	179	1.0	b
UGC 10669	Mailyan 97	Im?	34	16.15 ± 0.14	0.45 ± 0.08	-0.17 ± 0.08	3.54	440	52	1.5	d
UGC 10792	Mailyan 98	Im	54	15.92 ± 0.29	0.49 ± 0.04	-0.12 ± 0.10	8.70	1233	74	3.1	g
UGC 10805	DDO 207	SBm	31	14.62 ± 0.06	0.46 ± 0.05	-0.16 ± 0.10	7.30	1552	60	0.8	g
UGC 10991	VII Zw 741	Im	71	15.44 ± 0.08	0.31 ± 0.04	-0.39 ± 0.06	5.30	1465	91	1.2	g
	DDO 210	IB(s)m	68	13.93 ± 0.32	0.34 ± 0.06	-0.08 ± 0.11	15.18	-141	36	0.8	j
UGC 11755	NGC 7077	BCD/E	43	14.14 ± 0.04	0.50 ± 0.03	-0.18 ± 0.03	2.03	1155	158	0.1	k
UGC 11782		SB(s)m	53	13.83 ± 0.05	0.42 ± 0.04	-0.20 ± 0.06	10.92	1112	141	0.6	h
UGC 11944		Im:	71	14.92 ± 0.09	0.42 ± 0.03	-0.18 ± 0.07	12.78	1734	169	1.8	e
UGCA 433	DDO 215	Im:	46	15.20 ± 0.10	0.33 ± 0.06	-0.29 ± 0.10	7.77	829	82	1.4	d
UGC 12212		Sm:	47	14.60 ± 0.14	0.46 ± 0.04	-0.29 ± 0.06	15.30	892	113	1.6	g
UGCA 439	MK 324	BCD	36	15.20 ± 0.02	0.40 ± 0.03	-0.30 ± 0.03	2.34	1607	175	0.4	k
UGC 12613	DDO 216	ImV	70	12.20 ± 0.15	0.56 ± 0.04	-0.04 ± 0.09	29.90	-183	40	0.3	j
UGC 12713		S0/a	64	14.62 ± 0.03	0.46 ± 0.03	-0.16 ± 0.04	8.60	298	167	0.9	g
UGC 12894		Im	37	16.05 ± 0.20	...	...	6.24	335	57	2.5	f
Secondary Sample											
UGC 1924		Sd	84	14.89 ± 0.10	...	...	7.29	595	125	1.0	c
UGC 5423		Im	54	14.73 ± 0.10	...	...	3.32	349	67	0.4	f
UGC 5571		Sm:	69	15.73 ± 0.20	...	...	7.70	664	64	2.2	g
UGCA 292	CVn I dWA	ImIV-V	43	16.03 ± 0.05	...	...	17.60	309	45	6.9	j
UGC 8647		Im:	78	16.4 ± 1.0	...	...	5.12	747	77	2.9	h
UGC 8651	DDO 181	Im	53	14.43 ± 0.05	...	...	12.33	201	63	1.1	b
UGC 8760	DDO 183	Im	71	14.39 ± 0.05	...	...	10.04	189	45	0.9	d
UGC 8833		Im:	32	15.09 ± 0.05	...	...	5.33	225	38	0.9	d

Note. — Morphological type from the RC3. Inclination derived from the optical axial ratios, assuming  $q_0=0.2$ . All quantities have been corrected for Galactic Extinction. (a) HI parameters from van Zee et al. (1997d); widths re-measured at 20% of the peak. (b) HI parameters from Haynes et al. (1998); widths re-measured at 20% of the peak. (c) HI parameters from Giovanelli et al. (1997). (d) HI parameters from Fisher & Tully (1981). (e) HI parameters from Giovanelli & Haynes (1993). (f) HI parameters from Schneider et al. (1992). (g) HI parameters from Tift & Cocks (1988). (h) HI parameters from Schneider et al. (1990); flux corrected for pointing errors. (i) HI parameters from van Zee, in prep (VLA observations of the galaxy pair). (j) HI parameters from Young, van Zee, & Lo, in prep (VLA observations). (k) HI parameters from van Zee, Salzer, & Skillman, in prep (VLA observations).

Table 2. Derived Properties of the Isolated Dwarf Galaxy Sample

Galaxy Name	Dist. (Mpc)	$M_B$	$\mu_B^{0,c}$ (mag arcsec $^{-2}$ )	$\alpha$ (kpc)	$\nabla(B-V)$ (mag kpc $^{-1}$ )	$\nabla(U-B)$ (mag kpc $^{-1}$ )	Log $M_{HI}$ ( $M_\odot$ )	SFR ( $M_\odot$ yr $^{-1}$ )	$\langle SFR \rangle_{past}$ ( $M_\odot$ yr $^{-1}$ )	Log $\tau_g$ (yr)
Primary Sample										
UGC 191	17.60	-17.52	22.32	1.91	-0.05	-0.06	9.15	0.132	0.203	10.03
UGC 231	13.81	-17.13	26.74	2.20	-0.03	...	9.30	0.072	0.383	10.44
UGC 290	12.70	-14.48	24.91	1.14	+0.02	+0.06	8.40	0.0050	0.0047	10.70
UGCA 9	5.21	-14.17	23.11	0.62	+0.09	-0.00	7.62	0.0018	0.0052	10.35
UGCA 15	4.43	-12.93	23.17	0.38	+0.22	+0.19	7.32	<0.001	0.0010	>10.71
UGC 634	31.35	-17.67	23.13	2.89	-0.03	-0.04	9.57	0.073	0.144	10.71
UGC 685	5.5	-14.74	21.46	0.37	+0.36	+0.24	7.98	0.0077	0.015	10.09
UGC 891	10.52	-15.53	23.42	1.25	+0.00	+0.03	8.67	0.010	0.033	10.66
UGC 1104	11.11	-16.08	21.06	0.44	+0.22	+0.23	8.51	0.023	0.037	10.14
UGC 1175	11.32	-14.13	22.55	0.51	-0.04	-0.06	8.66	0.0032	0.0023	11.15
UGC 1281	4.58	-14.91	23.93	0.92	+0.00	+0.08	8.29	0.0084	0.014	10.36
UGC 1501	4.83	-16.27	22.64	1.28	+0.02	+0.07	8.58	0.042	0.042	9.96
UGC 2023	10.17	-16.54	22.82	1.57	-0.03	-0.10	8.62	0.072	0.074	9.76
UGC 2345	20.30	-17.33	22.69	2.38	+0.02	+0.02	9.36	0.107	0.129	10.33
UGC 2603	36.53	-18.38	22.68	3.86	-0.00	+0.00	9.44	0.400	0.196	9.84
UGCA 61	21.87	-17.92	24.46	4.12	-0.02	-0.03	9.61	0.333	0.167	10.09
UGC 3371	13.38	-16.92	24.21	3.65	-0.04	-0.06	9.07	0.092	0.233	10.10
UGC 3647	19.67	-17.06	21.79	1.44	+0.03	+0.09	9.17	0.150	0.098	9.99
UGC 3672	12.66	-15.43	22.62	0.87	+0.13	+0.11	8.76	0.014	0.008	10.63
UGC 4117	10.03	-14.86	22.57	0.58	+0.11	+0.11	8.10	0.010	0.006	10.12
UGC 4121	15.73	-15.90	24.36	1.97	-0.02	-0.02	8.97	0.028	0.048	10.52
UGC 4325	7.65	-16.70	22.16	1.25	-0.05	+0.01	8.58	0.058	0.072	9.82
UGC 5205	17.79	-16.29	22.13	0.92	+0.03	+0.07	8.78	<0.001	0.024	>12.65
CGCG 007-025	17.79	-15.75	20.53	0.37	-0.08	+0.51	8.62	0.115	0.022	9.56
UGC 5288	5.29	-14.44	20.57	0.23	+0.30	+0.70	8.23	0.0083	0.012	10.31
UGC 5414	8.23	-16.39	22.43	1.19	+0.02	+0.06	8.60	0.046	0.038	9.94
UGC 9128	2.5	-12.63	22.78	0.24	+0.53	+0.26	7.29	0.0001	0.0056	11.27
UGC 9211	10.92	-15.43	23.68	1.49	-0.12	-0.10	8.86	0.013	0.011	10.75
UGC 9219	10.40	-16.33	22.60	1.11	-0.06	-0.06	8.51	0.030	0.047	10.04
UGC 9240	3.74	-14.60	21.55	0.34	+0.27	+0.12	7.90	0.0035	0.0073	10.36
UGC 9500	22.63	-16.77	22.87	2.27	+0.01	+0.05	9.03	0.096	0.092	10.05
UGC 9992	8.61	-14.97	22.84	0.71	-0.04	+0.01	8.28	0.0062	0.010	10.48
UGC 10054	23.00	-18.13	22.02	2.28	-0.03	+0.00	9.38	0.169	0.291	10.15
UGC 10310	12.22	-16.81	22.63	1.78	-0.05	-0.06	8.84	0.123	0.064	9.76
UGC 10351	14.02	-16.06	21.35	0.59	+0.08	+0.12	8.64	0.022	0.040	10.30
UGC 10445	15.08	-17.53	21.79	1.49	-0.07	-0.10	9.20	0.162	0.159	9.99
UGC 10669	9.09	-13.65	23.76	0.69	-0.04	+0.02	7.84	<0.001	0.005	>11.31
UGC 10792	19.75	-15.56	23.87	1.25	-0.05	-0.10	8.90	0.013	0.040	10.80
UGC 10805	22.82	-17.17	21.81	1.20	-0.02	+0.03	8.95	0.124	0.152	9.86
UGC 10991	22.82	-16.35	22.85	1.46	-0.01	+0.08	8.81	0.036	0.025	10.26
DDO 210	0.95	-10.96	24.36	0.18	+0.49	+0.95	6.51	<0.00001	0.0002	>12.01
UGC 11755	18.03	-17.14	22.56	1.35	+0.27	+0.33	8.19	0.088	0.189	9.24
UGC 11782	17.97	-17.44	22.19	2.08	+0.00	+0.04	8.92	0.085	0.138	9.99
UGC 11944	26.48	-17.19	24.30	4.32	-0.01	-0.03	9.32	0.094	0.118	10.35
UGCA 433	13.27	-15.41	22.95	1.13	+0.05	+0.03	8.51	0.022	0.012	10.16
UGC 12212	15.46	-16.35	22.93	1.41	-0.05	-0.08	8.94	0.052	0.068	10.22
UGCA 439	24.37	-16.73	19.74	0.30	+0.44	+0.43	8.52	0.065	0.068	9.70
UGC 12613	0.76	-12.20	24.34	0.38	+0.29	+0.25	6.61	0.00003	0.0030	11.08
UGC 12713	7.53	-14.76	22.56	0.45	+0.30	+0.45	8.06	0.0093	0.016	10.09
UGC 12894	7.89	-13.38	23.02	0.42	...	...	7.96	0.0033	0.0014	10.45
Secondary Sample										
UGC 1924	9.95	-15.09	...	...	...	...	8.23	0.0048	0.013	10.55
UGC 5423	6.60	-14.36	...	...	...	...	7.53	0.0071	0.0056	9.68
UGC 5571	9.63	-14.19	...	...	...	...	8.23	0.0046	0.0057	10.56
UGCA 292	3.1	-11.43	...	...	...	...	7.60	0.0019	0.0004	10.32
UGC 8647	10.64	-13.71	...	...	...	...	8.14	0.0077	0.0035	10.25
UGC 8651	3.84	-13.49	...	...	...	...	7.63	0.0042	0.0031	10.01
UGC 8760	3.63	-13.41	...	...	...	...	7.49	0.0013	0.0027	10.39
UGC 8833	4.03	-12.94	...	...	...	...	8.14	0.0011	0.0018	10.27

Note. — All quantities have been corrected for Galactic Extinction.